MODELING SUCCESSIVE EXCAVATION WITHIN TWO DIMENSIONAL FINITE ELEMENT MESH

Tomáš JANDA *, Michal ŠEJNOHA and Jiří ŠEJNOHA

Department of Mechanics, Faculty of Civil Engineering, CTU in Prague, Thákurova 7, 166 29 Praha 6
*Corresponding author's e-mail: tomas.janda@fsv.cvut.cz

ABSTRACT

The study presents a modification to conventional finite element method under plane strain conditions to address the problem of successive excavation of linear parts of tunnels. Although the successive excavation is a three-dimensional mechanical problem, the designers often prefer 2D analysis owing to considerably simple and transparent geometric model and fast computations when compared to a 3D solution. The main idea behind the suggested method referred to as, 2D3D model, is to express the influence of excavation of a single stroke of soil not only in the particular cross section but in the entire soil body in front of and behind the examined profile. This is achieved by introducing special finite elements which have common triangular cross-section but are of infinite length in the longitudinal direction. The longitudinal approximations of the displacement field adopt the evolution of convergence measurements, while standard linear shape functions are kept in the element triangular cross-section. A profile corresponding to the city road tunnel Blanka in Prague with available convergence measurements was examined to verify the method. The results show that the method provides reasonably accurate results when compared to the convergence confinement method without the need to subjectively determine the lambda parameter. It also significantly reduces the computational time of a more versatile but complex 3D analysis.

KEYWORDS: excavation, finite element method, convergence measurements, convergence confinement method, plasticity, tunnel

TABLE INTRODUCTION

Dense urbanization accompanied by intensive traffic found in large cities often leads to major changes in traffic infrastructure. In many cases the only way to accommodate the traffic density is to place the road under already build-up area into a tunnel. In this regard the driven types of tunnels have a clear advantage over the cut-and-cover types since the driven tunnels, when designed and constructed properly, minimize the impact on the buildings and environment even during the construction. Nevertheless, the design strongly depends on a geological profile and material properties.

Therefore, a reliable tool capable of capturing the nonlinear behavior of soil material and also the structure of geological profile takes an important role in the design. Apart from simple analytical methods the civil engineer faces a choice between two-dimensional and three-dimensional finite element software.

The proposed modification, further referred to as 2D3D model, is designed to compute the settlements and stress and strain fields in the soil and internal forces in the primary lining. Similar to the convergence confinement method the 2D3D model is useful to effectively analyze the linear parts of the tunnel since it requires constant geometry along the tunnel axis and knowledge of the shape of the longitudinal convergence curves. The convergence curves are the result of standard monitoring during tunnel construction works. Convergence measurement procedure is described in detail in (Barták et al., 1998).

The necessity of knowing the shape of the convergence curves allows us to apply the method in two situations. In the stage of primary design the shape can be estimated based on the monitoring of other tunnels constructed in similar geological conditions. Furthermore, during the construction phase the method can be used to refine the design values or to quickly assess the possible variants addressing a non-standard response of the structure. In this case it will be advantageous to update the values of convergence curves obtained by monitoring a particular section. The model also makes it possible to relevantly describe the response of the soil environment to the excavation of one stroke and

therefore becomes an efficient tool to cope with the interaction between the tunnel itself and the upper-structure (Ebermann at al., 2010). Owning to its simplicity it appears to be an efficient tool to estimate the probability of failure of both the tunnel and the surface structure taking random properties of the soil environment into account (Šejnoha at al., 2011), (Špačková at al., 2010). An efficient and consistent introduction to the theory of structural reliability can be found in (Holický, 2009).

Currently, the method is extended for the use in conjunction with standard elastic plastic material models of soils. The model was tested with linearly elastic perfectly plastic Drucker-Prager material model neglecting hardening (Potts and Zdravkovič, 1999). The primary lining made of air-placed concrete (shotcrete) assumes a linear elastic behavior.

PRINCIPLES

Analyzing the successive excavation by finite element method under plane strain conditions consist of two computational steps. In the initial step the geostatic stress is computed and then in the second step, the excavated material is removed from the model and the excavation forces are applied which cause the tunnel profile to converge. In plane strain formulation this approach would correspond to excavating the whole tunnel in one stroke without applying the primary lining. This computation often leads to unrealistic large settlements or even to loss of stability if plastic material models are adopted. The other extreme case would be to install the primary lining prior to the second computational step. This would correspond to building first the primary lining in the untouched soil body and then excavating the whole tunnel tube in one stroke. This approach is again unrealistic and overestimates the internal forces in primary lining because it limits the ability of soils to create a natural vault above the profile. This disadvantage of plane strain conditions led to the formulation of convergence confinement method which keeps the 2D finite element geometry and addresses some of the observed phenomena of a successive excavation.

CONVERGENCE CONFINEMENT METHOD

When modeling the process of excavation under plane strain conditions the so called excavation forces acting at the nodes of the boundary separating the tunnel and surrounding soil are evaluated first based on the state of stress before excavation. Next, the excavated elements are removed and the boundary is loaded by excavation forces being directed inwards the tunnel. These forces induce the tunnel convergence, evolution of displacements throughout the examined area, terrain settlement and likely also the onset of plastic strains in critical regions.

In case of the New Austrian Tunneling Method the primary lining is constructed shortly after
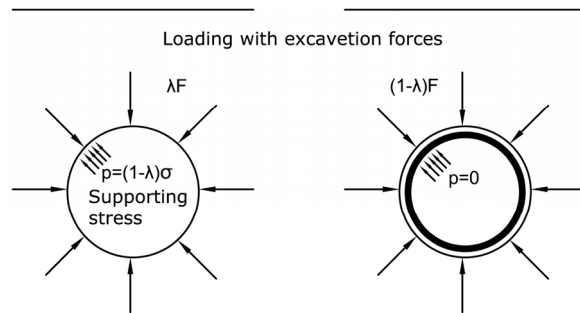

Fig. 1 Application of excavation forces in convergence confinement method.

performing excavation of a particular stroke. It is clear from excavation measurements that the soil body is already deformed at that time and, as the tunnel heading progresses, the deformation of the soil body-lining system grows further. The convergence confinement method (Panet and Guenot, 1982) models the development of deformations in a given cross-section by dividing the excavation forces in two parts. The first part is applied to an unsupported profile resulting in deformations that represent the state before the construction of lining. The remaining portion of excavation forces is applied to the excavated section already reinforced by the lining as displayed in Figure 1. The resulting deformations represent the final state, i.e. deformations at the time when the heading moved sufficiently far away from the analyzed section. Reducing the excavation forces acting on an unsupported tunnel allows this method to account for various spatial effects such as the supporting effect of material before heading or a longitudinal vault developed above the profile without lining. This part of excavation forces is determined by the parameter λ.

The advantage of the convergence confinement method is that it builds upon a 2D geometrical model, which is not only created much faster compared to a 3D model but it can also be easily checked. We also recall that the corresponding 2D finite element analysis considerably reduces the computational time.

Thus the principal task of the user is to determine the ratio of excavation forces being applied in the first and second calculation steps, i.e. determining the parameter λ. Since the value of this parameter cannot be impartially defined, engineers generally rely on empirical relations and their estimates. For practical application of this method the reader is referred to (Gramblička et al,. 2004) describing the analysis of the Turecký vrch railway tunnel. This particular analysis was performed using the GEO Tunnel software product (Šejnoha, 2009).

MODEL 2D3D

An alternative approach to the convergence confinement method is the proposed 2D3D model
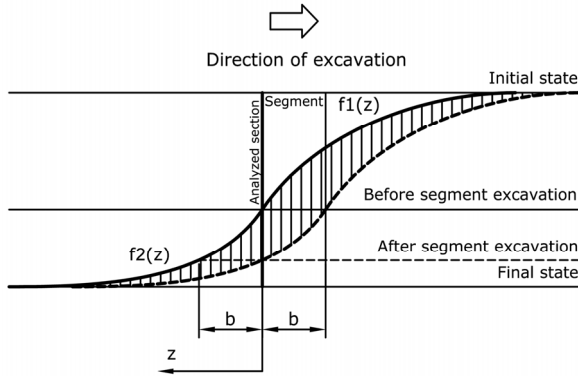
Fig. 2   Evolution of displacements caused by a single stroke.

which uses dimensional reduction from 3D space to 2D plane. The theoretical basis is described in (Janda et al., 2007). The model assumptions are similar to the convergence confinement method. The model requires a fixed geometry and material parameters along the longitudinal axis, which makes it suitable for solving linear quasi homogeneous sections of an underground structure.

Convergence extensometer measurements indicate that the deformation of the selected profile is closely related to the current location of the tunnel face. The settlement begins to occur when the tunnel face approaches the monitored profile and continues to grow. The settlement increases more rapidly when the tunnel face passes under the extesometric borehole. As the advancing tunnel face moves further the rate of growing settlements slows down and the settlements finally stabilize at their final values, see Figure 2.

In case of sufficiently long and homogeneous tunnel section it can be observed that the convergence curve (or longitudinal depression) does not change the shape or size and simply moves forward along with the excavation of each stroke. Knowing the shape of

the convergence curve we can determine how the excavation affects settlement not only in the examined cross-section but also in front of the tunnel face. Thus the principle of the 2D3D model is to analyze the projection of a single excavation step to the increment of displacements. The values of total displacements at any point are then obtained as the sum of the increments of displacements caused by the excavation of all individual strokes.

The finite elements of the 2D3D model have similar properties as the standard 2D triangular elements in its cross-section. In the direction of tunnel axis the elements are divided into three sections. The middle section represents the material that is excavated in one step. Neighboring semi-infinite sections represent the material in front of and behind this central section. A linear approximation of transverse displacements (i.e. displacement parallel to the x-y plane) is identical to standard three node triangular elements (Bittnar and Šejnoha, 1996). The longitudinal displacements are approximated by introducing a longitudinal shape function $f(z)$, which characterizes the effect of excavation of a single section. The shape of this function is draws upon analogy with the two-parametric Winkler-Pasternak subsoil model (Bittnar and Šejnoha, 1996). The function $f(z)$, see Figure3, is constant in the middle section and exponentially decreases in the outer sections

$$(z) = f_1(z) = \exp\left(\alpha^-\left(z + \frac{b}{2}\right)\right) \text{for } z \in \langle -\infty, -\frac{b}{2}\rangle \tag{1}$$

$$f(z) = 1 \text{ for } z \in \langle -\frac{b}{2}, \frac{b}{2}\rangle, \tag{2}$$

$$f(z) = f_2(z) = \exp\left(-\alpha^+\left(z - \frac{b}{2}\right)\right) \text{for } z \in \langle \frac{b}{2}, \infty\rangle, \tag{3}$$

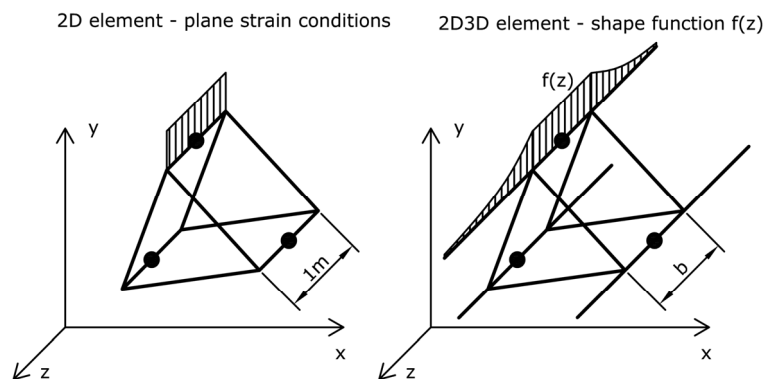where parameters α^+ and α^- are calibrated through

Fig. 3   Comparison between standard 2D and 2D3D element.

the convergence curves. Hence the shape functions $f(z)$ can differ in front of and behind the tunnel face and the corresponding parameters α are distinguished by superscripts referring to positive and negative directions of z-axis. Note that the analysis of a single excavated section must be preceded by the determination of initial stresses for the computation of excavation forces. This stress is calculated in two stages. In the first stage the initial geostatic stress is computed assuming simply the plane strain conditions. The next stage serves to estimate the stress distribution before performing the analysis of a single excavation step. The third then stage gives the desired increment of displacements caused by a single excavation step, which is decisive for the determination of the overall settlement. Introduction of elements modeling the soil and primary lining in individual stages is shown in Figure 3.

Analysis of practical problems requires the possibility of using at least basic elasto-plastic material models. The accurate expression of the evolution of plastic deformation outside the analyzed plane would need to introduce several finite sections in front of and behind the analyzed plane and proper computation of stresses in their integration points. This would shift the computational demands of the model near to the classical 3D model. In the present version of the proposed 2D3D model each of the three sections considers one integration point to evaluate both the stress increments and increments of plastic strains. Note that the increments of plastic strains in lateral sections are assumed proportional to the increments of total strains.

FINITE ELEMENTS FORMULATION

A new type of finite element was developed to describe the displacement, strain and stress fields not only in the solved cross-section but also outside this plane. The suggested formulation exploits the principles of isoparametric elements and thus allows for direct numerical integration. This approach requires introduction of natural coordinate system and the transformation relation between the natural and global coordinates.

In a general three-dimensional space the global and natural coordinates are stored in column vectors $\boldsymbol{x}$ and $\boldsymbol{x'}$, respectively.

$$\boldsymbol{x} = \begin{Bmatrix} x \\ y \\ z \end{Bmatrix}, \boldsymbol{x'} = \begin{Bmatrix} x' \\ y' \\ z' \end{Bmatrix}. \tag{4}$$

The transformation from natural to global coordinates $\boldsymbol{x'} \to \boldsymbol{x}$ is given by

$$\begin{aligned} x &= x_1 + (x_2 - x_1)x' + (x_3 - x_1)y', \\ y &= y_1 + (y_2 - y_1)x' + (y_3 - y_1)y', \\ z &= z', \end{aligned} \tag{5}$$

or in matrix form as

$$\boldsymbol{x} = \boldsymbol{A}\boldsymbol{x'} + \boldsymbol{b},$$
$$\begin{Bmatrix} x \\ y \\ z \end{Bmatrix} = \begin{bmatrix} x_2 - x_1 & x_3 - x_1 & 0 \\ y_2 - y_1 & y_3 - y_1 & 0 \\ 0 & 0 & 1 \end{bmatrix} \begin{Bmatrix} x' \\ y' \\ z' \end{Bmatrix} + \begin{Bmatrix} x_1 \\ y_1 \\ 0 \end{Bmatrix}, \tag{6}$$

where the values x_i and y_i denote the global coordinates of the i-th node which is fixed since the generated mesh does not change during the analysis. The inverse relation then reads

$$\boldsymbol{x'} = \boldsymbol{A}^{-1}(\boldsymbol{x} - \boldsymbol{b}). \tag{7}$$

The matrix $\boldsymbol{A}^{-1}$ is provided by

$$\boldsymbol{A}^{-1} = \begin{bmatrix} \frac{1}{J}(y_3 - y_1) & \frac{1}{J}(x_1 - x_3) & 0 \\ \frac{1}{J}(y_1 - y_2) & \frac{1}{J}(x_2 - x_1) & 0 \\ 0 & 0 & 1 \end{bmatrix}, \tag{8}$$

$$J = (x_2 - x_1)(y_3 - y_1) - (x_3 - x_1)(y_2 - y_1).$$

Note that the matrix $\boldsymbol{A}$ is the Jacobian matrix of the $\boldsymbol{x'} \to \boldsymbol{x}$ transformation while the matrix $\boldsymbol{A}^{-1}$ is the Jacobian matrix of the inverse transformation $\boldsymbol{x} \to \boldsymbol{x'}$

$$\frac{\partial \boldsymbol{x}}{\partial \boldsymbol{x'}} = \boldsymbol{A}, \ \frac{\partial \boldsymbol{x'}}{\partial \boldsymbol{x}} = \boldsymbol{A}^{-1}. \tag{9}$$

The linear shape functions expressed in terms of the natural coordinates for any point inside the element volume are given by

$$\begin{aligned} N_1 &= (1 - x' - y')f(z'), \\ N_2 &= x'f(z'), \\ N_3 &= y'f(z'), \end{aligned} \tag{10}$$

where $f(z')$ is exponentially decaying longitudinal function discussed later earlier, recall Eqs. (1)-(3). Displacements within the volume of a triangular three-node element are then described as

$$\boldsymbol{u} = \boldsymbol{N}(\boldsymbol{x'})\boldsymbol{r}, \tag{11}$$

$$\begin{Bmatrix} u \\ v \end{Bmatrix} = \begin{bmatrix} N_1 & 0 & N_2 & 0 & N_3 & 0 \\ 0 & N_1 & 0 & N_2 & 0 & N_3 \end{bmatrix} \begin{Bmatrix} u_1 \\ v_1 \\ u_2 \\ v_2 \\ u_3 \\ v_3 \end{Bmatrix}.$$

Derivatives of the shape functions with respect to the natural coordinates are written as

$$\frac{\partial \boldsymbol{N}}{\partial x\prime} = \begin{bmatrix} \frac{\partial N_1}{\partial x\prime} & \frac{\partial N_1}{\partial y\prime} & \frac{\partial N_1}{\partial z\prime} \\ \frac{\partial N_2}{\partial x\prime} & \frac{\partial N_2}{\partial y\prime} & \frac{\partial N_2}{\partial z\prime} \\ \frac{\partial N_3}{\partial x\prime} & \frac{\partial N_3}{\partial y\prime} & \frac{\partial N_3}{\partial z\prime} \end{bmatrix} = \begin{bmatrix} -f(z') & -f(z') & (1-x'-y')\frac{\partial f(z')}{\partial z\prime} \\ f(z') & 0 & x'\frac{\partial f(z')}{\partial z\prime} \\ 0 & f(z') & y'\frac{\partial f(z')}{\partial z\prime} \end{bmatrix}. \tag{12}$$

Next, applying the chain rule we write the derivatives with respect to the global coordinates in the form

$$\frac{\partial \boldsymbol{N}}{\partial x} = \frac{\partial \boldsymbol{N}}{\partial x\prime}\frac{\partial x\prime}{\partial x} = \begin{bmatrix} -f(z') & -f(z') & (1-x'-y')\frac{\partial f(z')}{\partial z'} \\ f(z') & 0 & x'\frac{\partial f(z')}{\partial z'} \\ 0 & f(z') & y'\frac{\partial f(z')}{\partial z'} \end{bmatrix} \begin{bmatrix} \frac{1}{J}(y_3-y_1) & \frac{1}{J}(x_1-x_3) & 0 \\ \frac{1}{J}(y_1-y_2) & \frac{1}{J}(x_2-x_1) & 0 \\ 0 & 0 & 1 \end{bmatrix} \tag{13}$$

$$= \begin{bmatrix} \frac{1}{J}(y_2-y_3)f(z') & \frac{1}{J}(x_3-x_2)f(z') & (1-x'-y')\frac{\partial f(z')}{\partial z'} \\ \frac{1}{J}(y_3-y_1)f(z') & \frac{1}{J}(x_1-x_3)f(z') & x'\frac{\partial f(z')}{\partial z'} \\ \frac{1}{J}(y_1-y_2)f(z') & \frac{1}{J}(x_2-x_1)f(z') & y'\frac{\partial f(z')}{\partial z'} \end{bmatrix}.$$

In a general 3D case the matrix $\boldsymbol{B}$ is expressed in terms of the matrix $\boldsymbol{N}$ and the operator matrix $\boldsymbol{\partial}^T$ such that

$$\boldsymbol{B} = \boldsymbol{\partial}^T \boldsymbol{N} = \begin{bmatrix} \frac{\partial}{\partial x} & 0 & 0 \\ 0 & \frac{\partial}{\partial y} & 0 \\ 0 & 0 & \frac{\partial}{\partial z} \\ 0 & \frac{\partial}{\partial z} & \frac{\partial}{\partial y} \\ \frac{\partial}{\partial z} & 0 & \frac{\partial}{\partial x} \\ \frac{\partial}{\partial y} & \frac{\partial}{\partial x} & 0 \end{bmatrix} \begin{bmatrix} N_1 & 0 & 0 & N_2 & 0 & 0 & N_3 & 0 & 0 \\ 0 & N_1 & 0 & 0 & N_2 & 0 & 0 & N_3 & 0 \\ 0 & 0 & N_1 & 0 & 0 & N_2 & 0 & 0 & N_3 \end{bmatrix} \tag{14}$$

Since the model allows displacements only parallel to the triangular cross-section, we can leave out the third column of the matrix $\boldsymbol{\partial}^T$ and the third row and every third column of the matrix $\boldsymbol{N}$ to arrive at

$$\boldsymbol{B} = \begin{bmatrix} \frac{\partial}{\partial x} & 0 \\ 0 & \frac{\partial}{\partial y} \\ 0 & 0 \\ 0 & \frac{\partial}{\partial z} \\ \frac{\partial}{\partial z} & 0 \\ \frac{\partial}{\partial y} & \frac{\partial}{\partial x} \end{bmatrix} \begin{bmatrix} N_1 & 0 & N_2 & 0 & N_3 & 0 \\ 0 & N_1 & 0 & N_2 & 0 & N_3 \end{bmatrix} = \begin{bmatrix} \frac{\partial N_1}{\partial x} & 0 & \frac{\partial N_2}{\partial x} & 0 & \frac{\partial N_3}{\partial x} & 0 \\ 0 & \frac{\partial N_1}{\partial y} & 0 & \frac{\partial N_2}{\partial y} & 0 & \frac{\partial N_3}{\partial y} \\ 0 & 0 & 0 & 0 & 0 & 0 \\ 0 & \frac{\partial N_1}{\partial z} & 0 & \frac{\partial N_2}{\partial z} & 0 & \frac{\partial N_3}{\partial z} \\ \frac{\partial N_1}{\partial z} & 0 & \frac{\partial N_2}{\partial z} & 0 & \frac{\partial N_3}{\partial z} & 0 \\ \frac{\partial N_1}{\partial y} & \frac{\partial N_1}{\partial x} & \frac{\partial N_2}{\partial y} & \frac{\partial N_2}{\partial x} & \frac{\partial N_3}{\partial y} & \frac{\partial N_3}{\partial x} \end{bmatrix}. \tag{15}$$

After expanding we obtain

$$B = \begin{bmatrix} \frac{y_2-y_3}{J}f & 0 & \frac{y_3-y_1}{J}f & 0 & \frac{y_1-y_2}{J}f & 0 \\ 0 & \frac{x_3-x_2}{J}f & 0 & \frac{x_1-x_3}{J}f & 0 & \frac{x_2-x_1}{J}f \\ 0 & 0 & 0 & 0 & 0 & 0 \\ 0 & (1-x'-y')\frac{\partial f}{\partial z'} & 0 & x'\frac{\partial f}{\partial z'} & 0 & y'\frac{\partial f}{\partial z'} \\ (1-x'-y')\frac{\partial f}{\partial z'} & 0 & x'\frac{\partial f}{\partial z'} & 0 & y'\frac{\partial f}{\partial z'} & 0 \\ \frac{x_3-x_2}{J}f & \frac{y_2-y_3}{J}f & \frac{x_1-x_3}{J}f & \frac{y_3-y_1}{J}f & \frac{x_2-x_1}{J}f & \frac{y_1-y_2}{J}f \end{bmatrix}, \tag{16}$$

The element stiffness matrix then takes the form

$$K = \int_{-\infty}^{\infty} \int_{A_e'} B^T(x')DB(x')J \, dx' \, dy' \, dz', \tag{17}$$

where standard Gaussian quadrature is employed to integrate the stiffness matrix in the transverse direction. For a three node triangular element this results in

$$K = \int_{-\infty}^{\infty} \frac{J}{2} B^T(1/3,1/3,z')DB(1/3,1/3,z') \, dz'. \tag{18}$$

A possible way to compute the inner part of the integral is to split the matrix B into two parts

$$B = fB_{xy} + \frac{\partial f}{\partial z'}B_z, \tag{19}$$

where the matrix B_{xy} contains only the derivatives with respect to x and y while the matrix B_z contains only the derivatives with respect to z. Hence

$$B_{xy} = \frac{1}{J}\begin{bmatrix} y_2-y_3 & 0 & y_3-y_1 & 0 & y_1-y_2 & 0 \\ 0 & x_3-x_2 & 0 & x_1-x_3 & 0 & x_2-x_1 \\ 0 & 0 & 0 & 0 & 0 & 0 \\ 0 & 0 & 0 & 0 & 0 & 0 \\ 0 & 0 & 0 & 0 & 0 & 0 \\ x_3-x_2 & y_2-y_3 & x_1-x_3 & y_3-y_1 & x_2-x_1 & y_1-y_2 \end{bmatrix}, \tag{20}$$

$$B_z = \begin{bmatrix} 0 & 0 & 0 & 0 & 0 & 0 \\ 0 & 0 & 0 & 0 & 0 & 0 \\ 0 & 0 & 0 & 0 & 0 & 0 \\ 0 & 1-x'-y' & 0 & x' & 0 & y' \\ 1-x'-y' & 0 & x' & 0 & y' & 0 \\ 0 & 0 & 0 & 0 & 0 & 0 \end{bmatrix}. \tag{21}$$

Now assume that the material stiffness matrix D is partitioned as

$$D = \begin{bmatrix} D_1 & D_2 & D_2 & 0 & 0 & 0 \\ D_2 & D_1 & D_2 & 0 & 0 & 0 \\ D_2 & D_2 & D_1 & 0 & 0 & 0 \\ 0 & 0 & 0 & D_3 & 0 & 0 \\ 0 & 0 & 0 & 0 & D_3 & 0 \\ 0 & 0 & 0 & 0 & 0 & D_3 \end{bmatrix}. \tag{22}$$

The above specific forms of matrices B_{xy}, B_z and D allows us to write

$$B^T DB = f^2 B_{xy}^T DB_{xy} + \left(\frac{\partial f}{\partial z'}\right)^2 B_z^T DB_z. \tag{23}$$

With the help of Eq. (23) the stiffness matrix (recall Eq. (18)) becomes

$$K = \int_{-\infty}^{\infty} \frac{J}{2}\left(f^2 B_{xy}^T DB_{xy} + \left(\frac{\partial f}{\partial z'}\right)^2 B_z^T DB_z\right) dz', \tag{24}$$

where the matrix $\boldsymbol{B}_z$ is expressed at one integration point [1/3,1/3]. Since the function $f(z')$ and its derivative are the only functions of z' we write the final form of the element stiffness matrix as

$$\boldsymbol{K} = \frac{J}{2}\boldsymbol{B}_{xy}^T\boldsymbol{D}\boldsymbol{B}_{xy}\int_{-\infty}^{\infty}f^2\,dz' + \frac{J}{2}\boldsymbol{B}_z^T\boldsymbol{D}\boldsymbol{B}_z\int_{-\infty}^{\infty}\left(\frac{\partial f}{\partial z'}\right)^2\,dz'. \tag{25}$$

Note that function f must be chosen a priori in order to yield the two integrals in Eq (25) finite. Finally, we write the vector of element nodal forces, again with the help of Gaussian quadrature, as

$$\boldsymbol{R} = \int_{-\infty}^{\infty}\boldsymbol{B}^T(1/3,1/3,z')\boldsymbol{\sigma}\,(1/3,1/3,z')\,dz\,. \tag{26}$$

The integration in the longitudinal direction can be obtained in a closed form analogically to the integration of element stiffness matrix. Each of the longitudinal sections of the element is assigned a single integration point and weight that corresponds to the integral over its length. The overall integral is computed as the sum of integrals over the three sections. This splitting is necessary to address the different load in the computational stages as shown in Figure 4.
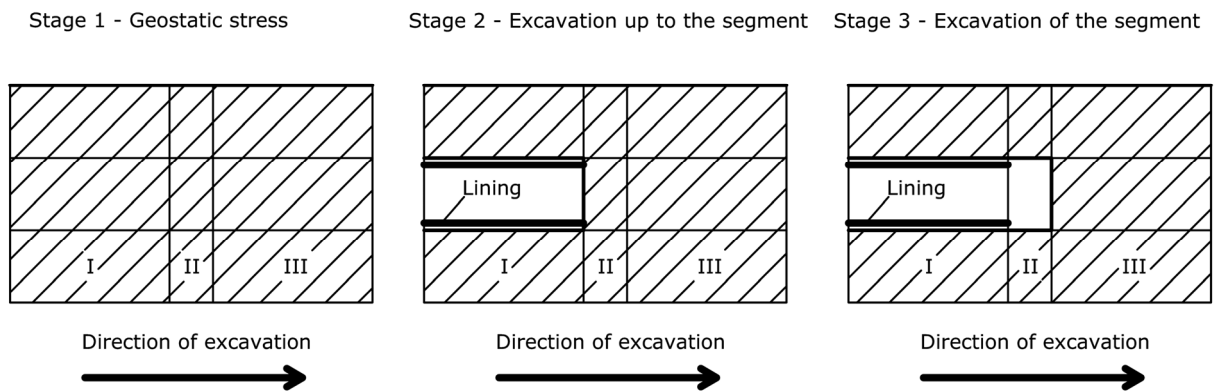

Fig. 4 Calculation stages.

ANALYZED EXAMPLE

In order to examine the behavior of the proposed 2D3D model a quasi-homogeneous sector No. 8 of the north tube of the Blanka road tunnel with available material data was considered. The geological profile consists of silt-clayey slate covered by fluvial sediments. The evolution of vertical displacements was monitored in an extensometric borehole situated above the tunnel. The borehole was equipped with four anchors in depths 9 m, 12 m, 15 m and 18.5 m. The deepest anchor was therefore located one meter above the tunnel crown. Particular arrangement of individual anchors is displayed in Figure 5. Figure 6 then shows the resulting settlement measured at anchor No. 4 depending on the position of a tunnel heading.

Convergence curves were used to calibrate the shape of longitudinal base functions in 2D3D finite elements. Since their actual magnitudes are irrelevant, the functions were normalized to ensure the continuity with the middle sections. Both functions $f_1(z)$ and $f_2(z)$ decay with a rate given by parameters α^+ and α^-, respectively. The higher the value of the exponent the faster the function decreases.

Convergence curves obtained by measuring the vertical displacements of anchors and terrain were fitted with the exponential curves proposed in the previous section. The values of exponents α^+ and α^- were found to graphically match the data as close as possible. The resulting approximation pertinent to anchor No. 4 is evident in Figure 6 showing quite accurate match with measurements. The distribution of exponents α^+ and α^- along the vertical line above the tunnel crown is plotted in Figure 7. Parameter α^-, which characterizes a gradual decay of the impact of excavation in front of the heading, tends to increase with depth from the value of 0.065 on the terrain to the value of 0.13 one meter above the tunnel crown. In order to assess the influence of its variation we performed the analysis first with the constant value of parameter $\alpha^- = 0.089$ obtained by averaging the measured values. Next, a certain variation of parameter α^- depending on depth was considered. In particular, until the depth of 17m (i.e. approximately one meter above the tunnel crown) the value of $\alpha^- = 0.079$ was used. Below this depth the value was assumed equal to $\alpha^- = 0.13$. However, this instant change in parameter α^- would result in the
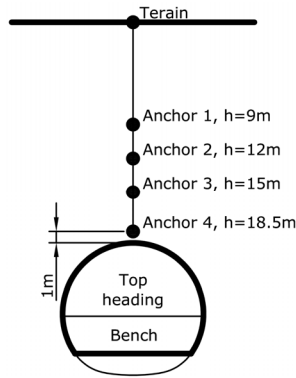
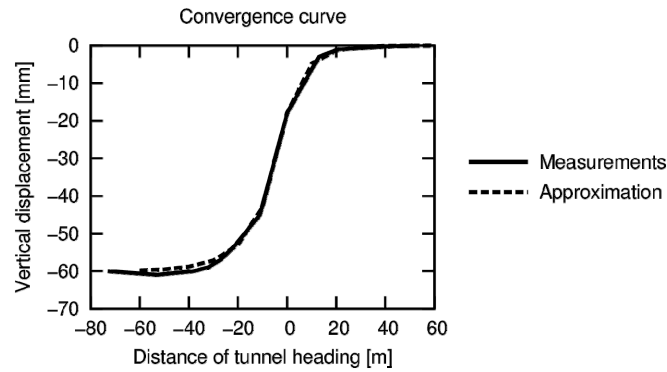**Fig. 5** Location of anchors in extensometric borehole.

Fig. 6 Comparison of measured convergence curve in anchor No. 4 and resulting approximation by exponential base functions.
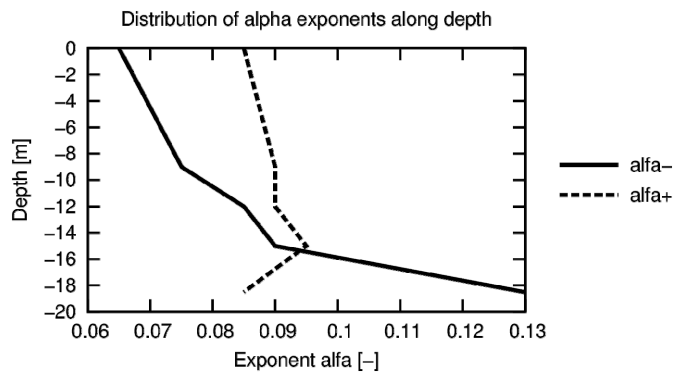

Fig. 7 Distribution of exponents α^+ and α^- derived from measurements.

incompatibility of displacements. If the parameter varied continuously in the vertical direction this incompatibility would not emerge. For simplicity and with reference to Fig. 7 we further adopted a constant value of $\alpha^+ = 0.089$ throughout the entire profile obtained again by averaging all measurements. Actual distributions of the exponent α^- employed in computations are displayed in Figure 8.

The geological profile is composed of three layers of fluvial sediments reaching up to the depth of 8.5 m. The tunnel itself was excavated in silt-clayey slate covered by these sediments. Both types of soils were represented by elastic plastic Drucker-Prager model with no strain hardening. The assumed material parameters for slate correspond to values recommended for a given region of the tunnel path. In particular, the value of self-weight equal to 24.5 kN/m, Poisson's number equal to 0.33, Young's modulus equal to 100 MPa, cohesion equal to 25 kPa, frictional angle equal to 28° and dilation angle equal to 0° were considered.

As for primary lining a linear elastic model was adopted. Parameters corresponding to concrete B25 with Young's modulus equal to 30 GPa and shear modulus equal to 12.5 GPa were used. The lining thickness equal to 150mm was introduced to support the upper (vault) region while the bottom region assumed no reinforcement. To represent the stiffening of lining at its base (elephant feet) preventing sinking of the two end points into the soil, we introduced two additional short beam elements perpendicular to the lining mid axis being directed into the soil body.

RESULTS

Since the convergence confinement method and the model of dimensional reduction 2D3D analyses a typical cross-section by different approach, only the total predicted settlements can be compared. Table 1 shows the final vertical displacements of the crown, invert and terrain. The presented values are computed adopting the 2D3D model with constant exponents α^- and α^+ and with exponent α^- depending on depth.
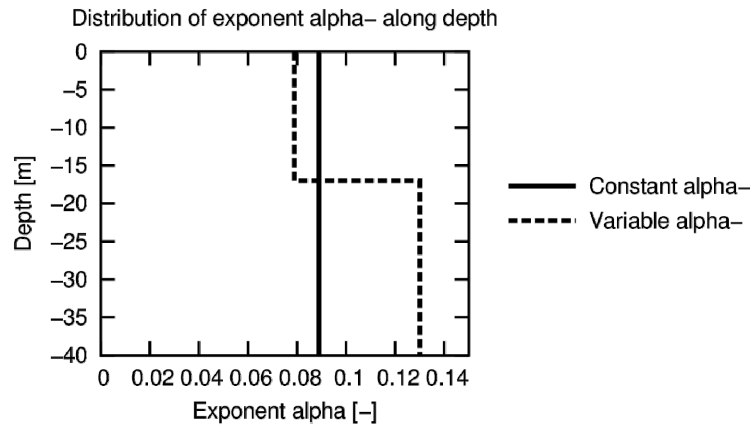
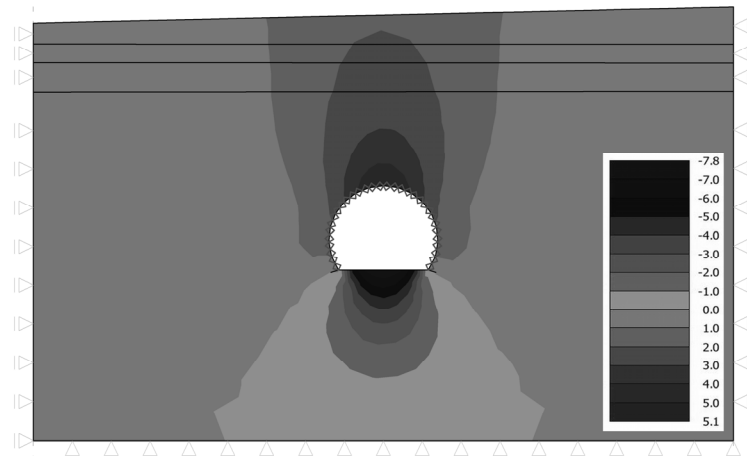**Fig. 8**   Distribution of exponent α^- used in computations.

Fig. 9   Distribution of increments of vertical displacements [mm] caused by excavation step.

Table 1 Comparison of settlement obtained with 2D3D model and convergence confinement method

Model	Model 2D3D, constant alfa-			Model 2D3D, variable alfa-			Convergence confinement		
Measured point	Crown	Terain	Invert	Crown	Terain	Invert	Crown	Terain	Invert
Increment of settlement [mm]	-5.80	-2.09	9.36	-5.26	-2.34	6.52	--	--	--
Total settlement [mm]	-70.70	-25.46	113.84	-67.71	-29.78	82.97	-62.62	-38.44	69.46

Further, the results computed using the convergence confinement method with coefficient $\lambda = 0.4$ are presented. This means that 40 % of excavation forces were applied to the unreinforced profile while the remaining 60 % were applied to the profile equipped with primary lining being the same as in the 2D3D model. Note that the parameter λ was chosen in order to match the measurements as close as possible. It is therefore an optimal choice. Figure 9 illustrates the distribution of increment of vertical settlement due to the excavation of one meter long stroke.

CONCLUSIONS

The suggested 2D3D model, developed on the principles of dimensional reduction, was examined in this paper through the example of application of the New Austrian Tunneling Method. Although the model takes into account the soil behavior in front of the tunnel heading and behind it, its finite mesh remains still two dimensional. The resulting vertical displacement of the tunnel crown given by the 2D3D model is 70.7 mm for the constant α^- and 67.7 mm when the value of α^- changes with depth. The value

of vertical displacement equal to 62.6 mm in the crown provided by the convergence confinement method is closer to the measured value of 61.2 mm. Note, however, that the value of the final settlement predicted by the convergence confinement method highly depends on the value of parameter λ which was assumed optimal in this study. On the contrary, the shapes of convergence curves, which serve to calibrate the longitudinal base functions of the 2D3D model, are defined uniquely based solely on field monitoring.

Similarity of the results of both variants of the 2D3D model – constant and variable exponent α^- – suggests that the computation is not very sensitive to detailed changes of longitudinal base functions above the tunnel. However, the distribution of the exponents α^- and α^+ bellow the tunnel may show more significant influence on the predicted displacement field. But this cannot be checked as the convergence curves are not constructed for this region. Inability to calibrate the element longitudinal base functions bellow the tunnel bottom might be one particular source for the explanation of more severe deviation of the displacement at the tunnel bottom predicted by the two methods.

The use of the 2D3D model may seem problematic from the practical point of view because its calibration requires convergence data that are not available when designing the structure. Nevertheless, this is not a major problem since the shape functions need only the knowledge of the shape of convergence curves for their calibration while the actual size is irrelevant. In the initial design, it is therefore possible to exploit convergence data known for other underground structures constructed in a similar geology. These predictions can be subsequently improved by implementing actual convergence data. Such a predictor-corrector approach would accommodate the two main advantages of the model: direct link to field monitoring and fast and transparent 2D computational model.

ACKNOWLEDGEMENT

REFERENCES

Barták, J., Macháček, J. and Pacovský, J.: 1998, Observation measuring of the earth-covered traffic tunnel structure in the quarry Hvížďalka. Tunel, No. 1, 6–9.

Bittnar, Z. and Šejnoha, J.: 1996, Numerical methods in structural engineering. ASCE Press and Thomas Telford Publ.

Ebermann, T., Hort, O., Křístek, V. and Rozsypal, A.: 2010, Deformations of ground surface and buildings caused by shallow tunnel excavation – Part 1. Tunel, No. 4, 4–14.

Šejnoha, M.: 2009, GEO FEM - Theoretical manual. http://www.fine.cz.

Gramblička, M, Šejnoha, M., Pruška, J.: 2004, The use of program geo fem for numerical modeling of tunnel Turecký vrch. Stavební obzor, No. 9, 265–271, (in Czech).

Holický, M.: 2009, Reliability analysis for structural design. Sun Media Stellenbosch.

Janda, T., Šejnoha, J. and Šejnoha, M.: 2007, Improved modeling of tunel excavation with two-dimensional finite elements. Proc. Recent Developments in Structural Engineering, Mechanics and Computations, Millpress, Rotterdam.

Panet, M. and Guenot, A.: 1982, Analysis of convergence behind the face of a tunnel. Proc. Tunnelling 82, London, 197–204.

Potts, D.M. and Zdravkovič, L.: 1999, Finite element analysis in geotechnical engineering – theory, Thomas Telford, London.

Šejnoha, J., Novotná, E., Špačková, O. and Jarušková, D.: 2011, Pragmatic probabilistic models for quantification of tunnel excavation risk, submitted to Acta Geodyn. Geomater.

Špačková, O., Ebermann, T., Kostohryz, O., Veselý, V. and Šejnoha, J.: 2010, Expert estimation of probability of failure during tunnel excavation. Tunel, No. 4, 15–23.